Protonation and Hydrogen-Bonding State of the Distal Histidine in the CO Complex of Horseradish Peroxidase As Studied by Ultraviolet Resonance Raman Spectroscopy†

Shinji Hashimoto*,‡ and Hideo Takeuchi§

Faculty of Science and Engineering, Tokyo University of Science, Yamaguchi, Daigaku Dori, Sanyo Onoda, Yamaguchi 756-0884, Japan, and Graduate School of Pharmaceutical Sciences, Tohoku University, Aobayama, Sendai 980-8578, Japan

Received March 9, 2006; Revised Manuscript Received June 6, 2006

ABSTRACT: Ultraviolet resonance Raman (UVRR) spectroscopy has been used to characterize the structure and hydrogen bonding state of the distal histidine (His42) in horseradish peroxidase (HRP) complexed with carbon monoxide (HRP−CO). The HRP−CO − HRP UVRR difference spectrum in D_2O solution at pD 7.0 shows two positive peaks at 1408 and 1388 cm^{-1}, which are ascribable to medium-to-weak and strong hydrogen bonding states, respectively, of the protonated imidazolium side chain of His42 in HRP−CO. Both His42 peaks decrease in intensity with increase of pD with a midpoint of transition at pD 8.8, indicating that the pK_a of His42 in HRP−CO is 8.8. The CO ligand exhibits two C−O stretching Raman peaks at 1932 and 1902 cm^{-1}, the latter of which diminishes at alkaline pD and is assignable to a strong hydrogen-bonded state. It is most probable that the imidazolium side chain of His42 forms a strong hydrogen bond with CO, giving a His42 peak at 1388 cm^{-1} and a CO peak at 1902 cm^{-1}, in one conformer. The other hydrogen bonding state of His42, giving the 1408 cm^{-1} peak, is ascribed to another conformer forming a medium-to-weak hydrogen bond with a water molecule in the distal cavity. The present finding that His42 can act as a strong proton donor to CO and decrease the CO bond order is consistent with the role of His42 as a general acid to cleave the O−O bond of hydrogen peroxide, a specific oxidizing agent, in the catalytic cycle of HRP.

Horseradish peroxidase (HRP)[1] is a 44-kDa glycoprotein enzyme (E.C. 1.11.1.7) that contains iron protoporphyrin IX as a heme prosthetic group. The enzyme catalyzes the oxidation of a wide variety of aromatic substrates by use of hydrogen peroxide (H_2O_2) as a specific oxidizing agent (*1*−*3*). The catalytic cycle of HRP is initiated by binding of H_2O_2 to the ferric heme iron (Fe^{3+}) from the distal side of the heme. Subsequently, heterolytic cleavage of the O−O bond of H_2O_2 occurs in conjunction with two-electron oxidation of the heme, resulting in the formation of an intermediate, compound **I**, which comprises an oxo-ferryl (Fe^{4+}═O) center and a porphyrin π cation radical. In the next step, compound **I** is converted to a second intermediate, compound **II**, by a single-electron transfer from a substrate to the porphyrin. Compound **II** is then converted back to the ferric state by another single-electron heme reduction coupled with substrate oxidation. All the chemical reactions occur in the cavity on the distal side, and the architecture of the distal cavity is important for understanding the catalytic mechanism of HRP. Chemical modification (*4*) and mutagenesis (*5*−*8*) studies have shown that two residues in the distal cavity, Arg38 and His42, are essential for the formation of compound **I**. Currently, these two distal residues are considered to assist the heterolytic cleavage of H_2O_2 through hydrogen bonding (*9*−*12*).

Carbon monoxide (CO) is a useful probe of the heme pocket structure because vibrational wavenumbers of the Fe-bound CO ligand are sensitive to interactions with residues on the distal side as well as to the nature of the Fe axial ligand on the proximal side (*13*). CO binds to HRP in the ferrous (Fe^{2+}) state, and the binary complex is stable enough to allow spectroscopic examination. IR absorption spectra of the CO-bound HRP (HRP−CO) have revealed two distinct CO stretch (ν_{CO}) bands at 1933 and 1905 cm^{-1} in neutral H_2O solution, the latter of which disappears in alkaline solution with a midpoint of transition at pH 8.7, while the former gains intensity (*14*−*16*). This observation indicates that there is a pH-dependent equilibrium between two CO binding modes. A combined analysis of the ν_{CO} IR bands and visible resonance Raman bands of the Fe−C stretching and Fe−C−O bending modes has shown that the 1933 cm^{-1} ν_{CO} mode is assignable to a conformer with a linear Fe−C−O linkage oriented perpendicularly to the heme plane, while the 1905 cm^{-1} mode is ascribed to another conformer also having a linear Fe−C−O linkage but tilted from the

† This work was supported by Grants-in-Aid for Scientific Research (No. 15550021 to S.H.) from the Japan Society for the Promotion of Science.

* To whom correspondence should be addressed. Phone: +81-836-88-4532. Fax: +81-836-88-3844. E-mail: shinji@ed.yama.tus.ac.jp.

‡ Tokyo University of Science, Yamaguchi.

§ Tohoku University.

[1] Abbreviations: HRP, horseradish peroxidase; HRP−CO, carbon monoxide complex of HRP; HRP−CN, cyanide complex of HRP; UVRR, ultraviolet resonance Raman; FTIR, Fourier transform infrared; ν_{CO}, C−O stretch; $\nu_{C4=C5}$, C_4═C_5 stretch of imidazole or imidazolium; ν_{NCN}, N_π−C−N_τ symmetric stretch of imidazolium; MeIm, 4-methylimidazole; $MeImD_2^+$, *N*-deuterated 4-methylimidazolium.

10.1021/bi060466f CCC: $33.50
Published on Web 07/20/2006

heme plane normal (*17*, *18*). The ν_{CO} wavenumber of the tilted conformer (1905 cm^{-1}) is much lower than that of the perpendicular conformer (1933 cm^{-1}), suggesting that CO forms a strong hydrogen bond with a proton donor in the tilted conformation but a weak one in the perpendicular conformation.

The transition of CO vibrational bands at pH 8.7 is analogous to a transition at pH 8.3 observed for the heme Soret absorption band of HRP−CO, which is ascribed to protonation/deprotonation of a residue in the vicinity of the heme (*19*). Thus, the transition between the two Fe−C−O conformers with different hydrogen bonding strength revealed by IR and Raman spectroscopy may be associated with protonation/deprotonation of a residue with a p$K_a \approx$ 8.5 in the vicinity of the heme. The residue having a p$K_a \approx$ 8.5 was proposed to be His42 because the corresponding alkaline transition disappeared in the His42 → Leu mutant (*20*, *21*). A simple interpretation of these findings is that the protonated imidazole (cationic imidazolium) ring of His42 directly forms a strong hydrogen bond with CO in the tilted conformer to give a ν_{CO} band at 1905 cm^{-1} as proposed in previous studies (*15*, *17*, *18*). Such a strong hydrogen bond would be disrupted upon deprotonation from His42 at alkaline pH. Alternatively, it is also conceivable that the positively charged guanidinium group of Arg38 forms a strong hydrogen bond with CO in the tilted conformer, whose stability is indirectly controlled by the protonation/deprotonation of the His42 imidazole ring (*20*, *21*). The latter interpretation is based on the observation that the His42 → Leu mutant, where Arg38 is conserved, gives a ν_{CO} band at a lower wavenumber and with a higher sensitivity to the H_2O → D_2O solvent change than the Arg38 → Leu mutant (*20*, *21*). These two interpretations are both plausible, and it is still inconclusive which of Arg38 and His42 is strongly hydrogen-bonded with CO in the tilted conformation. To resolve this problem, experimental evidence is required for the hydrogen bonding states of Arg38 and/or His42. Also needed is information about the pK_a of His42. Since the distal Arg and His residues are invariant in peroxidases, the hydrogen bonding scheme in the distal cavity of HRP is important for understanding the catalytic mechanism of peroxidases (*9*−*12*, *22*, *23*).

Ultraviolet resonance Raman (UVRR) spectroscopy is a useful tool for probing the protonation and hydrogen bonding states of His (*24*−*29*). Although the UVRR scattering from the imidazole ring of His is considerably weaker than that from the aromatic side chains of Tyr and Trp, it is still possible to observe the Raman bands of His with UV excitation when the protein does not contain many residues of Trp, the strongest UVRR scatterer among the amino acids. In particular, the *N*-deuterated imidazolium ring of His gives a relatively strong UVRR band around 1410 cm^{-1}, which can be used as a maker of His protonation (deuteronation) and hydrogen bonding (*24*, *28*). Fortunately, HRP contains only one Trp residue, and His42 is expected to be protonated/deprotonated at neutral/alkaline pH, thus, opening the possibility of UVRR determination of the pK_a and hydrogen bonding state of His42 in HRP−CO. In a previous UVRR study, we succeeded in detecting Raman signals of His42 in a cyanide complex of HRP (HRP−CN) (*24*). In this study, we have established that the pK_a of His42 is 8.8 and the protonated imidazole (imidazolium) side chain of His42 is strongly hydrogen-bonded with CO in HRP−CO.

EXPERIMENTAL PROCEDURES

Materials. HRP was purchased form Wako Chemicals Co. as lyophilized salt-free powder and purified on a carboxymethyl cellulose (Whatman CM52) column according to the method of Shannon et al. (*30*). The enzyme-rich fractions were dialyzed against deionized water and lyophilized. The final product contained predominantly isoenzyme C with a trace of isoenzyme B as judged from the column elution profile (*30*). Spectroscopic measurements were made for samples with an RZ value (ratio of the absorbance at 402 and 280 nm) of 3.0 or higher at pH 6.0.

Deuterium oxide (99.9% atom D) and 4-methylimidazole (MeIm) were obtained from Aldrich Co. MeIm was decolorized by charcoal followed by three-times recrystallization from water as a nitrate salt. The organic solvents used to dissolve MeIm were γ-butyrolactone, acetone, pyridine, *N*,*N*-dimethylformamide, *N*,*N*-dimethylacetamide, dimethyl sulfoxide, triethyl phosphate, and hexamethylphosphoric triamide. The solvents were dehydrated with standard methods before use. *N*-deuterated 4-methylimidazolium ($MeImD_2^+$) was obtained by lyophilizing the acidic D_2O solution of MeIm. All other chemicals were of the highest grade available and used without further purification.

Preparation of Samples. The lyophilized enzyme powder was dissolved in 50 mM buffer solution at a concentration of 160 μM. The buffers used were sodium phosphate (pH 7), Tris-HCl (pH 8−9), and glycine (pH > 9). The concentration of HRP was determined by using the extinction coefficient of the Soret absorption band at 403 nm, $\epsilon_{403} = 1.02 \times 10^5\ M^{-1}\ cm^{-1}$ (*31*). All sample solutions contain 100 mM Na_2SO_4 as a Raman intensity standard. Prior to preparation of D_2O solution, the enzyme was lyophilized from D_2O to ensure complete exchange of labile protons. The pD values reported are direct pH meter readings.

The CO adduct of HRP was prepared as follows. Carbon monoxide was gently flowed over the surface of the ferric HRP solution at 0 °C. The enzyme was then reduced by the addition of an anaerobically prepared dithionite solution. The enzyme solution became bright red upon reduction and CO-binding, and it was allowed to stand under the CO atmosphere for 30 min. At pH 6.0, the CO complex gave two ν_{CO} IR bands as reported previously, confirming the presence of two conformers (*16*).

Spectral Measurements. UV Raman spectra were excited at 244 nm by using continuous-wave radiation from an intracavity, frequency-doubled Ar^+ ion laser (Coherent Innova 300 FReD) and recorded on a fore-prism UV Raman spectrometer (*32*) equipped with a liquid nitrogen-cooled CCD detector (Princeton Instruments LN/CCD-1752). The sample solution was circulated by a peristaltic pump from a 15-mL reservoir through a quartz capillary. The solutions were prevented from being exposed to atmospheric oxygen during the Raman measurement. The laser beam (~5 mW at the sample point) was focused on the sample stream in the capillary tube in a backscattering geometry. Typically, Raman spectra were recorded with an accumulation time of ~100 min, and three or more spectra recorded on fresh samples were averaged. The sample integrity was checked

by comparing the first and last 20-min UVRR spectra for each sample. A slight UV-induced conversion from HRP−CO to HRP was noticed. However, such conversion decreased only the overall intensity of the difference spectrum HRP−CO − HRP and did not change the shape of the spectrum nor affect the interpretation of the difference spectrum. Wavenumber calibration was effected by using the Raman spectrum of a cyclohexanone−acetonitrile mixture (1:1, v/v), and peak wavenumbers of sharp Raman bands were reproducible to within ±1 cm^{-1}.

Visible Raman spectra were recorded on a JASCO NR1800 Raman spectrometer equipped with a CCD detector (Princeton Instruments LN/CCD-1152). Excitation was provided by a 514.5-nm line (100 mW at the sample point) from an Ar^+ ion laser (Spectra Physics Stabilite 2017). The spectrometer was calibrated by using emission lines from a neon lamp. The reproducibility of peak wavenumbers were better than ±1 cm^{-1}.

UV−visible absorption spectra were recorded on a Hitachi U-3400 spectrophotometer. A Fourier transform infrared (FTIR) spectrophotometer (JEOL JIR-WINSPEC50) was used to measure IR spectra.

RESULTS

The 244-nm-excited resonance Raman spectrum of HRP−CO at pH 7.0 is shown in Figure 1a. The protein contains five Tyr residues (at positions 7, 185, 201, 233, and 234) and one Trp residue (at position 117) (*33*), and the spectra are dominated by Tyr and Trp Raman bands, which are denoted with Y and W, respectively. The intensities of these Tyr and Trp bands are about 3−4 times stronger than those of aqueous aromatic amino acids (spectra not shown). Analogous UVRR intensity enhancement in protein environments has been observed for other proteins and ascribed to hydrogen bonding of the aromatic side chains as a proton donor under hydrophobic environments (*34*−*36*). The environmental hydrophobicity of the Trp117 side chain is also reflected in the relative intensity of a pair of W7 bands at 1358 and 1337 cm^{-1}, which serves as a hydrophobic interaction marker (*37*). The W7 intensity ratio (I_{1358}/I_{1337}) of ferric HRP is larger than that of aqueous amino acid Trp (*34*), suggesting a hydrophobic environment of the Trp117 side chain. The wavenumber of the W3 band (1548 cm^{-1}) is known to be sensitive to the dihedral angle, $|\chi^{2,1}|$, about the bond connecting the indole ring with the C_β atom of Trp (*38*). According to the correlation between the W3 wavenumber and the dihedral angle (*38*), the 1548 cm^{-1} band indicates that the $|\chi^{2,1}|$ angle of Trp117 is about 90°. The UVRR spectrum also exhibits scattering from the peptide main chain. The amide I (mainly carbonyl stretch) band is seen at 1662 cm^{-1}, consistent with the predominantly α-helical structure revealed by X-ray crystallographic analysis (*39*). A band peaking at 1454 cm^{-1} is assignable to the imide II mode of 17 Pro residues (*40*). In contrast to the strong Raman bands due to Tyr and Trp side chains, Raman bands of His side chains are too weak to be identified in the UVRR spectrum.

To find a clue to His Raman signals, we have subtracted the 244-nm-excited resonance Raman spectrum of ferric HRP (Figure 1b) from that of HRP−CO (Figure 1a). The difference spectrum is expected to reflect protein structural

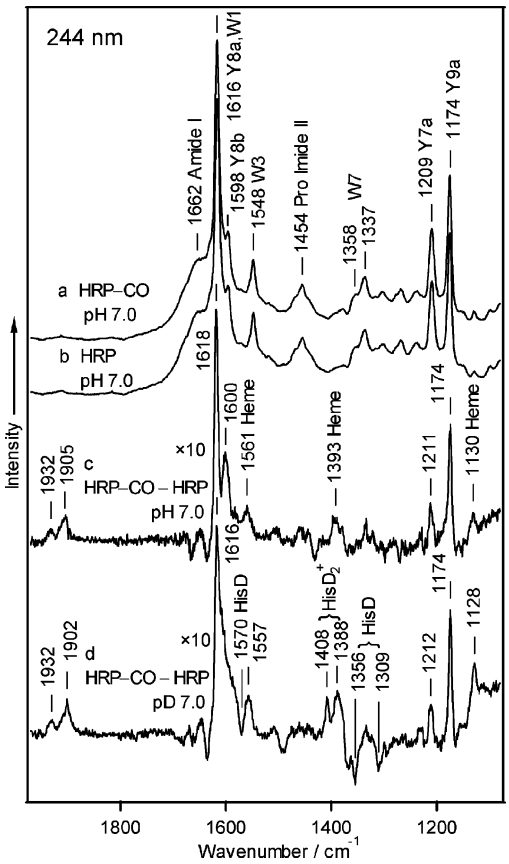

FIGURE 1: UV (244 nm) resonance Raman spectra of (a) HRP−CO and (b) ferric HRP in H_2O, and the difference spectra HRP−CO − HRP in (c) H_2O and (d) D_2O solution. The enzyme was dissolved at a concentration of 160 μM in 50 mM phosphate buffer (pH or pD 7.0) containing 100 mM Na_2SO_4 (an internal Raman intensity standard). Raman bands due to Tyr and Trp are indicated with W and Y, respectively, followed by vibrational mode numbers. The intensity scale of the difference spectra is expanded by a factor of 10.

changes induced by the reduction of the heme iron from Fe^{3+} to Fe^{2+} and subsequent ligation of CO. Such difference spectra in H_2O and D_2O solutions at pH (pD) 7.0 are shown in Figure 1c and d, respectively, after intensity enlargement by a factor of 10. In the H_2O solution (Figure 1c), positive peaks are seen at 1932, 1905, 1618, 1600, 1561, 1393, 1211, 1174, and 1130 cm^{-1}. The two bands at 1932 and 1905 cm^{-1} correspond well to the ν_{CO} IR bands reported previously (*14*−*16*), both in peak position and relative intensity, confirming the presence of two Fe−C−O conformers in HRP−CO. This observation demonstrates that UVRR spectroscopy is useful in detecting the ν_{CO} mode as is IR spectroscopy. The utility of UVRR spectroscopy in detecting heme ligand vibrations has also been reported for NO adducts of some heme proteins (*41*).

Four positive peaks at 1618, 1600, 1211, and 1174 cm^{-1} are assignable to Tyr, which gives strong UVRR bands at corresponding wavenumbers as seen in the original Raman spectra of HRP−CO and HRP (Figure 1a,b). Since the Tyr UVRR intensity increases with increase of hydrophobic interaction and increase of hydrogen bonding strength (*35*), the Tyr positive peaks are ascribable to an increase in either or both of these factors upon ligation of CO. Of the remaining three positive peaks, the 1393 cm^{-1} peak is assigned to heme skeletal vibrations characteristic of HRP−CO (*18*). The 1130

cm^{-1} peak is assigned to the heme C_β−vinyl stretch mode (*42*), which was also seen in a UVRR difference spectrum between HRP−CN and HRP (both ferric) (*24*). The ligand binding is likely to change the structure of the C_β−vinyl moiety and enhance the vinyl UVRR band. The origin of the 1561 cm^{-1} peak is unknown at present, but it could be tentatively assigned to a heme vibration because a weak Raman band is seen around 1560 cm^{-1} in visible resonance Raman spectra of HRP−CO (*18*).

The HRP−CO − HRP difference spectrum in D_2O solution at pD 7.0 (Figure 1d) also exhibits some peaks arising from CO (1932 and 1902 cm^{-1}), Tyr (1616, 1212, and 1174 cm^{-1}), and the heme (1557 and 1128 cm^{-1}). The 3-cm^{-1} downshift of the low-wavenumber component of the ν_{CO} doublet from 1905 to 1902 cm^{-1} in D_2O is consistent with the IR result (*15*), suggesting a significant proton motion associated with the ν_{CO} vibration due to a strong hydrogen bond between the CO ligand and a proton donor. In addition, the solvent change from H_2O to D_2O produces new difference signals: positive peaks at 1408 and 1388 cm^{-1} and negative peaks at 1570, 1356, and 1309 cm^{-1}. The positive peak at 1408 cm^{-1} is assigned to the N_π−C−N_τ symmetric stretch (ν_{NCN}) band of the *N*-deuterated imidazolium side chain of His (*28*, *43*). The emergence of this positive peak indicates that the pK_a of a His residue is high in HRP−CO compared to HRP, and the population of the imidazolium form significantly increases upon CO binding at pD 7. HRP contains three His residues, His40, His42, and His170. In the crystal structures of HRP (*39*) and HRP−CO (*10*), His170 is the proximal ligand of the heme iron and cannot become imidazolium at neutral pH. His40 is away from the heme and unlikely to be sensitive to the CO binding to the heme iron. Thus, His42 in the distal pocket must be the His residue whose pK_a is affected by the CO binding. The positive peak at 1408 cm^{-1} is therefore assigned to the ν_{NCN} mode of the *N*-deuterated imidazolium side chain of His42.

To assign the remaining peaks characteristic of the D_2O solution, we have examined the pD dependence of the difference spectrum. Panel A of Figure 2 shows UVRR difference spectra of HRP−CO − HRP at pD 7.0−9.4. The positive peaks arising from Tyr residues (1616, 1212, and 1174 cm^{-1}) persist over the pD range, indicating that the environmental hydrophobicity and hydrogen bonding strength of the Tyr side chains are not much affected by pD, at least in the pD range examined. On the other hand, the intensity of the ν_{CO} band at 1902 cm^{-1} decreases as the pD value increases from 7.0 to 9.4. The intensity decrease of the 1902 cm^{-1} ν_{CO} Raman band corresponds well to the pH titration behavior of the 1905 cm^{-1} ν_{CO} IR band in H_2O solution (*16*), indicating a loss of the tilted and strongly hydrogen-bonded Fe−C−O conformer at alkaline pH.

The 1408 cm^{-1} band of His42 also decreases in intensity with increase of pD as shown in panel B of Figure 2, where the intensity of the 1408 cm^{-1} band relative to the 1174 cm^{-1} Tyr band is plotted as a function of pD. The plot is well-approximated by a titration curve representing a single-H^+ dissociation with a pK_a value of 8.8, indicating that the pK_a of His42 in HRP−CO is 8.8. Very similar pD dependence is seen for the intensities of the positive peak at 1388 cm^{-1} and three negative peaks at 1570, 1356, and 1309 cm^{-1}. This

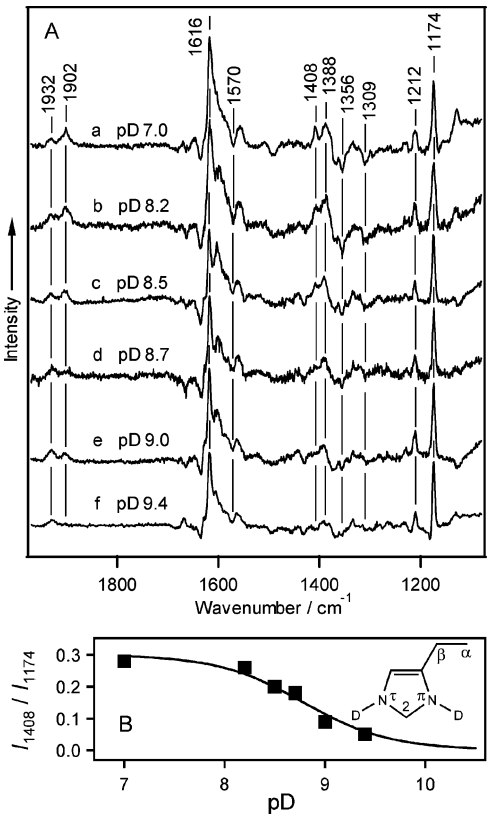

FIGURE 2: (A) UVRR difference spectra of HRPCO − HRP in D_2O buffer at the pD values indicated. (B) Plot of the relative intensity I_{1408}/I_{1174} as a function of pD. The solid line represents a theoretical curve for a single-H^+ dissociation with a pK_a value of 8.8.

observation strongly suggests that the four peaks are also associated with His42.

The 1388 cm^{-1} positive peak is downshifted by 20 cm^{-1} from the 1408 cm^{-1} positive peak of the ν_{NCN} mode of *N*-deuterated imidazolium side chain of His42. Since the *N*-deuterated imidazolium ring does not have normal vibrations other than ν_{NCN} around 1390 cm^{-1} (*44*), the 1388 cm^{-1} band may also be ascribed to ν_{NCN} of His42. To study the structural origin of this downshift, we have examined the effects of hydrogen bonding on the Raman bands of *N*-deuterated 4-methylimidazolium ($MeImD_2^+$), a model compound of the cationic His side chain. The model compound was dissolved in eight organic solvents that can act as hydrogen bonding acceptors. The visible Raman difference spectra, $MeImD_2^+$ − $MeImH_2^+$, in the organic solvents are shown in Figure 3. The strong Raman bands of solvents are canceled out in the spectra, and the positive and negative peaks are ascribed to $MeImD_2^+$ and $MeImH_2^+$, respectively. The wavenumbers of positive Raman bands around 1605 (C_4=C_5 stretch, $\nu_{C4=C5}$) and 1405 cm^{-1} (ν_{NCN}) are plotted in Figure 4 as a function of the β-scale, a parameter representing the hydrogen bond acceptor basicity (*45*). These two bands show downshifts by 3 and 6 cm^{-1}, respectively, with increase of the β-scale of the solvent from 0.46 (medium-strength hydrogen bonding) to 1.00 (strong hydrogen bonding). Therefore, the large (20 cm^{-1}) downshift of the ν_{NCN} mode in HRP−CO may partly be ascribed to a strong hydrogen bond. Another factor that might affect the ν_{NCN} wavenumber is the torsional angle about the C_α−C_β−C_4=C_5 linkage ($\chi^{2,1}$). The ν_{NCN} wavenumbers in five *N*-

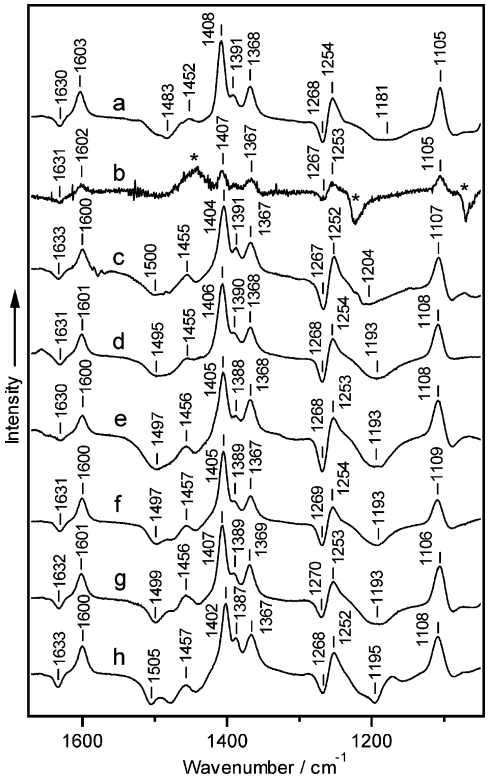

FIGURE 3: Raman difference spectra, $MeImD_2^+ - MeImH_2^+$, in proton-accepting solvents excited at 514.5 nm. The solvents used are (a) γ-butyrolactone, (b) acetone, (c) pyridine, (d) *N*,*N*-dimethylformamide, (e) *N*,*N*-dimethylacetamide, (f) dimethyl sulfoxide, (g) triethyl phosphate, and (h) hexamethylphosphoric triamide. The bands marked with * in (b) are due to uncompensated solvent acetone.

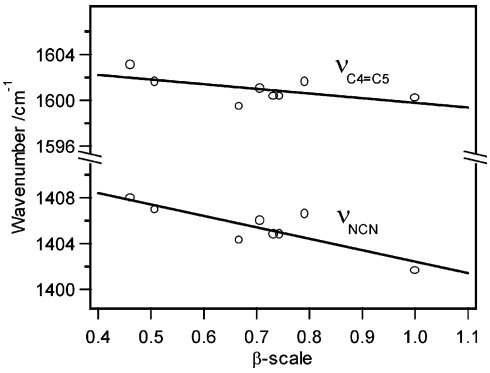

FIGURE 4: Plots of the wavenumbers of Raman bands of $MeImD_2^+$ as a function of the solvent β-scale parameter. The solvent β-scale values are 0.46 (γ-butyrolactone), 0.51 (acetone), 0.67 (pyridine), 0.71 (*N*,*N*-dimethylformamide), 0.73 (*N*,*N*-dimethylacetamide), 0.74 (dimethyl sulfoxide), 0.79 (triethyl phosphate), and 1.00 (hexamethylphosphoric triamide). The solid line indicates a least-squares fit with a straight line.

deuterated His crystals showed a dependence on the absolute value of the $\chi^{2,1}$ angle: an 8 cm^{-1} downshift on going from $|\chi^{2,1}| = 107°$ to 62° (*46*). In addition to an increase in hydrogen bonding strength, a decrease in $|\chi^{2,1}|$ would cause a further downshift of ν_{NCN}, totaling up to 20 cm^{-1}. It is likely that the 1408 cm^{-1} ν_{NCN} mode, which corresponds to that usually observed for amino acid His in acidic D_2O solution (*28*, *43*), may be ascribed to a conformer of His42 having a sterically stable $|\chi^{2,1}|$ value of ~90° and a medium-to-weak hydrogen bond. The 1388 cm^{-1} ν_{NCN} peak, on the other hand, may arise from another conformer of His42 having a small $|\chi^{2,1}|$ and a strong hydrogen bond with the heme ligand CO. The $\nu_{C4=C5}$ bands of both conformers are expected around 1600 cm^{-1} but are overlapped by a strong band at 1616 cm^{-1} due to Tyr (Figures 1 and 2).

Since the negative peaks at 1570, 1356, and 1309 cm^{-1} in the HRP−CO − HRP difference spectra show pD dependence similar to that observed for the positive peaks at 1408 and 1388 cm^{-1} due to His42 in HRP−CO (Figure 2, panel A), these negative peaks may also be ascribed to His42, not in HRP−CO but in HRP. If the pK_a of His42 in HRP is significantly lower than 7 as suggested previously (*47*), it is possible that the imidazole ring of His42 is not protonated in HRP at pD 7 and Raman bands of the neutral imidazole ring appear as negative peaks in the difference spectrum. A recent UVRR study on the tautomerism of neutral His in D_2O solution has discovered two pairs of tautomer marker bands in the 1400−1300 cm^{-1} region (*29*). The tautomer that carries a deuteron on the imidazole N_τ atom (N_τ-D) gives two Raman bands around 1380 and 1330 cm^{-1}, while the other tautomer having a deuteron on the N_π atom (N_π-D) gives bands around 1350 and 1310 cm^{-1}. The 1356 and 1309 cm^{-1} negative peaks in the HRP−CO − HRP difference spectrum (Figure 1d) are assigned to the latter pair of tautomer markers, indicating that His42 in HRP takes the N_π-D form but not the N_τ-D form. The negative peak at 1570 cm^{-1} may be assigned to the $\nu_{C4=C5}$ mode of His42 in HRP (*29*).

DISCUSSION

In this study, we have examined the UVRR spectrum of the CO complex of HRP (HRP−CO) in the ferrous state with special attention to the protonation and hydrogen bonding states of the distal His (His42). The Raman spectrum and its difference from that of uncomplexed ferric HRP provide structural information not only on His but also on Tyr and Trp residues. To correlate the UVRR spectral observations with protein structure, we have examined the crystal structure of a recombinant protein of HRP in the CO-bound ferrous state (Figure 5, Protein Data Bank, entry code 1W4Y) (*10*).

Conformation and Environment of Trp117. In the crystal structure of HRP−CO (*10*), the single Trp (Trp117) is located near the surface of the protein (15 Å away from the heme iron). The indole ring of Trp117 is surrounded by the hydrophobic CH_3 and CH_2 groups of Gln106, Val119, and Val278 side chains. Additionally, the indole N−H site is hydrogen-bonded to the carboxyl oxygen atom ($O_{\delta1}$) of Asp282 at a distance of 3.0 Å. The structure of the protein around Trp117 is consistent with the strong UVRR scattering (Figure 1a) characteristic of a Trp residue hydrogen-bonded in a hydrophobic environment (*36*). The $|\chi^{2,1}|$ angle of the Trp side chain in the crystal (103°) is close to that (90°) derived from the W3 UVRR wavenumber (*38*). Since the UVRR difference spectra between HRP−CO and HRP does not exhibit any change of Trp bands (Figure 1c,d), the CO ligand binding must not affect the protein structure around Trp117.

Hydrogen Bonding of Tyr233. The Tyr UVRR bands gain intensity on going from HRP to HRP−CO (Figure 1c,d). Of five Tyr residues in HRP, four are located away from the heme and unlikely to be affected by the reduction of the

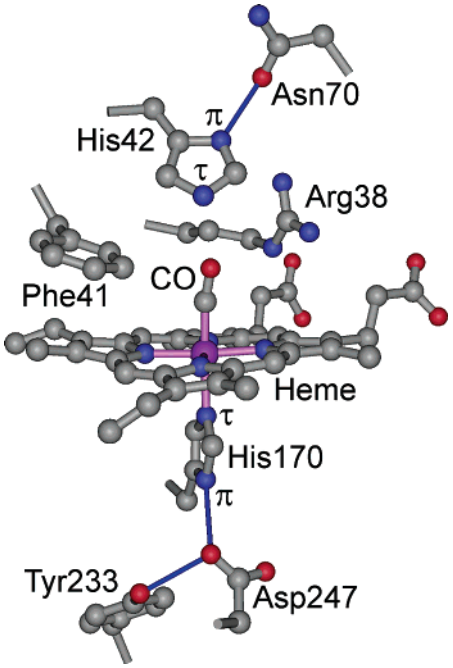

FIGURE 5: The active site structure of recombinant HRP−CO in the crystalline state. The atomic coordinates are taken from the Protein Data Bank (entry code 1ATJ, ref *10*). Key residues are shown on the distal (Phe41, His42, Arg38, and Asn70) and proximal (His170, Tyr233, and Asp247) sides of the heme.

heme iron or the ligation of CO. The remaining one Tyr residue (Tyr233) is located on the proximal side of the heme (Figure 5). The phenolic oxygen of the Tyr233 side chain is hydrogen-bonded with the $O_{\delta 1}$ atom of Asp247, which is accepting a hydrogen atom from the N_{π} atom of the Fe-bound proximal His (His170) as well (Figure 5). It has been proposed that strong attraction of the His170 N_{π} proton by Asp247 induces strong imidazolate character of His170, resulting in a stabilization of higher oxidation states of the heme iron (*48*, *49*). On going from HRP to HRP−CO, the heme iron is reduced from ferric (Fe^{3+}) to ferrous (Fe^{2+}). Accordingly, the imidazolate character of His170 in HRP−CO need not be so strong as in ferric HRP, and the donation of a proton from His170 to Asp247 may also be weakened. Instead, the $O_{\delta 1}$ atom of Asp247 would attract more strongly the phenolic O−H of Tyr233. The intensity increase of Tyr UVRR bands in HRP−CO may be ascribed to such an increase of the strength of hydrogen bonding of Tyr233 to Asp247 upon reduction of the heme iron. In other words, the present UVRR data support the stabilization mechanism of the heme oxidation state by hydrogen bonding on the proximal side (*48*, *49*).

pK_a and Hydrogen Bonding of His42 in HRP−CO. The pH profile of the 1408 cm^{-1} band intensity (Figure 2, panel B) shows that the pK_a of His42 in HRP−CO is 8.8, which is not much different from that (7.4) of the ligand-free form in the same ferrous state (*20*). In the ferric state, on the other hand, the pK_a of His42 is largely reduced to ∼4 in the ligand-free form (*47*) or elevated to ∼12 in the complex with CN^- (*24*). These observations suggest that the pK_a value of His42 is sensitive to the electric charge distribution in the Fe-ligand moiety. Compared with the ferrous state, the additional Fe positive charge in the ferric state would disfavor the protonated cationic form of His42 to decrease the pK_a to ∼4, while the negatively charged CN^- ligand located near His42 in HRP−CN^- is likely to stabilize the His42 cationic form, resulting in the large elevation of the pK_a to ∼12. Since the pK_a of His42 in HRP−CO is not much deviated from the physiological pH and protonation/deprotonation of His42 can easily occur as supposed for the complex with the specific oxidizing agent H_2O_2 (*10*), HRP−CO may be a good model for studying the role of His42 as a general acid−base catalyst.

IR absorption and visible resonance Raman spectra of HRP−CO revealed the presence of two conformers of the Fe−C−O linkage, each having a high (1933 cm^{-1}) or low (1905 cm^{-1}) ν_{CO} mode (*14*−*18*). The low-ν_{CO} conformer, which disappeared above pH 8.7, was supposed to have a strong hydrogen bond with a distal residue, His42 (*15*, *17*, *18*) or Arg38 (*16*). In this study, we have determined the pK_a of His42 to be 8.8 by using UVRR spectroscopy. The substantial coincidence of the His42 pK_a value and the midpoint pH value of the low-ν_{CO} conformer disappearance strongly suggests that His42 is the distal residue that forms a strong hydrogen bond with CO. This proposal is further supported by the finding that His42 exhibits a ν_{NCN} band at 1388 cm^{-1}, indicative of strong hydrogen bonding at imidazole nitrogen atoms. In previous studies (*20*, *21*), the CO ligand was proposed to form a strong hydrogen bond with Arg38 because the His42 → Leu mutant gave a ν_{CO} band at a lower wavenumber than the Arg38 → Leu mutant. Since Arg38 and His42 are in close proximity to each other (Figure 5), mutation of one of the two distal residues might cause a significant change in orientation and hydrogen bonding of the other residue.

In the crystal structure of HRP−CO (*10*), only the side chains of Arg38, Phe41, and His42 are close to the CO ligand, which perpendicularly sticks out from the heme plane (Figure 5). The Phe41 side chain does not form a hydrogen bond and cannot be a proton donor to CO. Arg38 has a guanidinium group containing three hydrogen bond donor nitrogens. However, the N−H hydrogen atoms point away from the CO ligand, and no hydrogen bond is conceivable between them. The imidazole N_{π} atom of His42 is hydrogen-bonded with the side chain carbonyl group of Asn70 on the wall of the distal cavity. The other imidazole nitrogen atom, N_{τ}, of His42 points to a water molecule, but not to the oxygen atom of the CO ligand. Therefore, the CO ligand has no apparent hydrogen bonding partner in the crystal structure. The high-ν_{CO} conformer with a medium-to-weak hydrogen bond may be alike that found in the crystal.

For the CO ligand to form a hydrogen bond with His42, the Fe−C−O linkage needs to be tilted (Figure 5). A different tilting of the Fe−C−O linkage makes it possible for CO to form a hydrogen bond with the $N_{\eta 2}$ atom of Arg38. Accordingly, the CO ligand can form a hydrogen bond with both of His42 and Arg38, if the Fe−C−O linkage is tilted from the heme plane normal. Since the Fe−C−O linkage is tilted in the low-ν_{CO} conformer (*17*, *18*), the CO ligand is likely to be hydrogen-bonded with His42 or Arg38. The present UVRR study has shown that His42 in HRP−CO takes two hydrogen bonding states, one giving a ν_{NCN} band at 1408 cm^{-1} and the other at 1388 cm^{-1}. The former medium-to-weak hydrogen bonding state of His42 corresponds to the high-ν_{CO} perpendicular conformer in the crystal structure. On the other hand, the latter strong hydrogen bonding state of His42 corresponds to the low-ν_{CO} tilted

conformer that would be seen only in solution. The presence of a strong hydrogen bond between His42 and the CO ligand is one of the novel findings of this study. The largely downshifted CO stretch wavenumber (1905 cm^{-1} in H_2O solution) in the tilted conformer indicates a decrease in CO bond order due to a strong back-bonding, an electron transfer from the heme iron to CO π^* orbitals (*13*). The present observation that His42 can act as a strong proton donor to the CO ligand and diminish the CO bond order is consistent with the role of His42 as a general acid in the heterolytic cleavage of the O−O bond of H_2O_2 bound to HRP (*10*).

REFERENCES

1. Dunford, H. B. (1999) *Heme Peroxidases*, Wiley-VCH, New York.
2. English, A. M., and Tsaprailis, G. (1995) Catalytic structure−function relationships in heme peroxidases, *Adv. Inorg. Chem. 43*, 79−125.
3. Veitch, N. C., and Smith, A. T. (2001) Horseradish peroxidase, *Adv. Inorg. Chem. 51*, 107−162.
4. Bhattacharyya, D. K., Bandyopadhyay, U., and Baneriee, R. K. (1992) Chemical and kinetic evidence for an essential histidine in horseradish peroxidase for Iodide oxidation, *J. Biol. Chem. 267*, 9800−9804.
5. Newmyer, S. L., and Ortiz de Montellano, P. R. (1995) Horseradish peroxidase His-42 → Ala, His-42 → Val, and Phe-41 → Ala mutants. Histidine catalysis and control of substrate access to the heme iron, *J. Biol. Chem. 270*, 19430−19438.
6. Rodriguez-Lopez, J. N, Smith, A. T., and Thorneley, R. N. F. (1996) Recombinant horseradish peroxidase isoenzyme C: the effect of distal haem cavity mutations (His42 → Leu and Arg38 → Leu) on compound I formation and substrate binding, *J. Biol. Inorg. Chem. 1*, 136−142.
7. Rodriguez-Lopez, J. N., Smith, A. T., and Thorneley, R. N. F. (1996) Role of arginine 38 in horseradish peroxidase; a critical residue for substrate binding and catalysis, *J. Biol. Chem. 271*, 4023−4030.
8. Tanaka, M., Ishimori, K., Mukai, M., Kitagawa, T., and Morishima, I. (1997) Catalytic activities and structural properties of horseradish peroxidase distal His42 → Glu or Gln mutant, *Biochemistry 36*, 9889−9898.
9. Poulos, T. L., and Kraut, J. (1980) The stereochemistry of peroxidase catalysis, *J. Biol. Chem. 255*, 8199−8205.
10. Carlsson, G. H., Nicholls, P., Svistunenko, D., Berglund, G. I., and Hajdu, J. (2005) Complexes of horseradish peroxidase with formate, acetate, and carbon monoxide, *Biochemistry 44*, 635−642.
11. Rodriguez-Lopez, J. N., Lowe, D. J., Hernandez-Ruiz, J., Hiner, A. N. P., Garcia-Canovas, F., and Thorneley, R. N. F. (2001) Mechanism of reaction of hydrogen peroxide with horseradish peroxidase: identification of intermediates in the catalytic cycle, *J. Am. Chem. Soc. 123*, 11838−11847.
12. Henriksen, A., Smith, A. T., and Gajhede, M. (1999) The structures of the horseradish peroxidase C-ferulic acid complex and the ternary complex with cyanide suggest how peroxidases oxidize small phenolic substrates, *J. Biol. Chem. 274*, 35005−35011.
13. Spiro, T. G., and Wasbotten, I. H. (2005) CO as a vibrational probe of heme protein active sites, *J. Inorg. Biochem. 99*, 34−44.
14. Barlow, C. H., Ohlsson, P.-I., and Paul, K.-G. (1976) Infrared spectroscopic studies of carbonyl horseradish peroxidases, *Biochemistry 15*, 2225−2229.
15. Smith, M. L., Ohlsson, P.-I., and Paul, K. G. (1983) Infrared spectroscopic evidence of hydrogen bonding between carbon monoxide and protein in carbonyl horseradish peroxidase C, *FEBS Lett. 163*, 303−305.
16. Holzbaur, I. E., English, A. M., and Ismail, A. A. (1996) Infrared spectra of carbonyl horseradish peroxidase and its substrate complexes: characterization of pH-dependent conformers, *J. Am. Chem. Soc. 118*, 3354−3359.
17. Evangelista-Kirkup, R., Smulevich, G., and Spiro, T. G. (1986) Alternative carbon monoxide binding modes for horseradish peroxidase studied by resonance Raman spectroscopy, *Biochemistry 25*, 4420−4425.
18. Uno, T., Nishimura, Y., Tsuboi, M., Makino, R., lizuka, T., and Ishimura, Y. (1987) Two types of conformers with distinct Fe−C−O configuration in the ferrous CO complex of horseradish peroxidase. Resonance Raman and infrared spectroscopic studies with native and deuteroheme-substituted enzymes, *J. Biol. Chem. 262*, 4549−4556.
19. Hayashi, Y., Yamada, H., and Yamazaki, I. (1976) Heme-linked proton dissociation of carbon monoxide complexes of myoglobin and peroxidase, *Biochim. Biophys. Acta 427*, 608−616.
20. Rodriguez-Lopez, J. N., George, S. J., and Thorneley, R. N. F. (1998) The structure of carbonyl horseradish peroxidase: spectroscopic and kinetic characterization of the carbon monoxide complexes of His-42 → Leu and Arg-38 → Leu mutants, *J. Biol. Inorg. Chem. 3*, 44−52.
21. Feis, A., Rodriguez-Lopez, J. N., Thorneley, R. N. F., and Smulevich, G. (1998) The distal cavity structure of carbonyl horseradish peroxidase as probed by the resonance Raman spectra of His42Leu and Arg38Leu mutants, *Biochemistry 37*, 13575−13581.
22. Miller, M. A., Shaw, A., and Kraut, J. (1994) 2.2 Å structure of oxy-peroxidase as a model for the transient enzyme: peroxide complex, *Nat. Struct. Biol. 1*, 524−531.
23. Berglund, G. I., Carlsson, G. H., Smith, A. T., Szdke, H., Menriksen, A., and Hajdu, J. (2002) The catalytic pathway of horseradish peroxidase at high resolution, *Nature 417*, 463−468.
24. Hashimoto, S., and Takeuchi, H. (1998) Detection of UV resonance Raman bands of the distal histidine in cyanide-bound horseradish peroxidase: evidence for two hydrogen bonding states of the imidazolium side chain, *J. Am. Chem. Soc. 120*, 11012−11013.
25. Zao, X., Wan, D., and Spiro, T. G. (1998) A UV resonance Raman monitor of histidine protonation in proteins: Bohr protons in hemoglobin, *J. Am. Chem. Soc. 120*, 8517−8518.
26. Okada, A., Miura, T., and Takeuchi, H. (2001) Protonation of histidine and histidine−tryptophan interaction in the activation of the M2 ion channel from influenza a virus, *Biochemistry 40*, 6053−6060.
27. Wu, Q., Li, F., Wang, W., Hecht, M. H., and Spiro, T. G. (2002) UV Raman monitoring of histidine protonation and H-^{2}H exchange in plastocyanin, *J. Inorg. Biochem. 88*, 381−387.
28. Takeuchi, H. (2003) Raman structural markers of tryptophan and histidine side chains in proteins, *Biopolymers 72*, 305−317.
29. Toyama, A., Takahashi, Y., and Takeuchi, H. (2004) Catalytic and structural role of a metal-free histidine residue in bovine Cu−Zn superoxide dismutase, *Biochemistry 43*, 4670−4679.
30. Shannon, L. M., Kay, E., and Lew, J. Y. (1965) Peroxidase isozymes from horseradish roots. I. Isolation and physical properties, *J. Biol. Chem. 241*, 2166−2172.
31. Dunford, H. B., and Stillman, J. S. (1976) On the function and mechanism of action of peroxidases, *Coord. Chem. Rev. 19*, 187−251.
32. Hashimoto, S., Ikeda, T., Takeuchi, H., and Harada, I. (1993) Utilization of a prism monochromator as a sharp-cut bandpass filter in ultraviolet Raman spectroscopy, *Appl. Spectrosc. 47*, 1283−1285.
33. Welinder, K. G. (1979) Amino acid sequence studies of horseradish peroxidase. Amino and carboxyl termini, cyanogen bromide and tryptic fragments, the complete sequence, and some structural characteristics of horseradish peroxidase C, *Eur. J. Biochem. 96*, 483−502.
34. Hashimoto, S., Miura, K., Yamagishi, T., Takeuchi, H., and Harada, I. (1992) Ultraviolet resonance Raman study on purple and blue membranes of *Halobacterium halobium*, *Photochem. Photobiol. 56*, 1097−1103.
35. Hashimoto, S., Yabusaki, T., Takeuchi, H., and Harada, I. (1995) Structure and ligand-binding modes of human serum albumin studied by UV resonance Raman spectroscopy, *Biospectroscopy 1*, 375−385.
36. Matsuno, M., and Takeuchi, H. (1998) Effects of hydrogen bonding and hydrophobic interactions on the ultraviolet resonance Raman intensities of indole ring vibrations, *Bull. Chem. Soc. Jpn. 71*, 851−857.
37. Harada, I., Miura, T., and Takeuchi, H. (1986) Origin of the doublet at 1360 and 1340 cm^{-1} in the Raman spectra of tryptophan and related compounds, *Spectrochim. Acta 42A*, 307−312.
38. Miura, T., Takeuchi, T., and Harada, I. (1989) Tryptophan Raman bands sensitive to hydrogen bonding and side-chain conformation, *J. Raman Spectrosc. 20*, 667−671.
39. Gajhede, M., Schuller, D. J., Henriksen, A., Smith, A. T., and Poulos, T. L. (1997) Crystal structure of horseradish peroxidase C at 2.15 Å resolution, *Nat. Struct. Biol. 4*, 1032−1038.

40. Takeuchi, H., and Harada, I. (1990) Ultraviolet resonance Raman spectroscopy of X-proline bonds: a new marker band of hydrogen bonding at the imide C=O site, *J. Raman Spectrosc. 21*, 509−515.
41. Tomita, T., Haruta, N., Aki, M., Kitagawa, T., and Ikeda-Saito, M. (2001) UV resonance Raman detection of a ligand vibration on ferric nitrosyl heme proteins, *J. Am. Chem. Soc. 123*, 2666−2667.
42. De Vito, V. L., and Asher, S. A. (1989) UV resonance Raman enhancement of vinyl stretching in ferric protoporphyrin IX: conjugation and preservation of the vinyl $\pi \rightarrow \pi^*$ transition, *J. Am. Chem. Soc. 111*, 9143−9152.
43. Tasumi, M., Harada, I., Takamatsu, T., and Takahashi, S. (1982) Raman studies of L-histidine and related compounds in aqueous solution, *J. Raman Spectrosc. 12*, 149−151.
44. Hasegawa, K., Ono, T., and Noguchi, T. (2000) Vibrational spectra and ab initio DFT calculations of 4-methylimidazole and its different protonation forms: infrared and Raman markers of the protonation state of a histidine side chain, *J. Phys. Chem. B 104*, 4253−4265.
45. Kamlet, M. J., and Taft, R. W. (1976) The solvatochromic comparison method. I. The β-scale of solvent hydrogen-bond acceptor (HBA) basicities, *J. Am. Chem. Soc. 98*, 377−383.
46. Takeuchi, H., Kimura, Y., Koitabashi, I., and Harada, I. (1991) Raman bands of *N*-deuterated histidinium as markers of conformation and hydrogen bonding, *J. Raman Spectrosc. 22*, 233−236.
47. Araiso, T., and Dunford, H. B. (1980) Horseradish peroxidase. XLI. Complex formation with nitrate and its effect upon compound I formation, *Biochem. Biophys. Res. Commun. 94*, 1177−1182.
48. De Ropp, J. S., Thanabal, V., and La Mar, G. N. (1985) NMR evidence for a horseradish peroxidase state with a deprotonated proximal histidine, *J. Am. Chem. Soc. 107*, 8268−8270.
49. De Ropp, J. S., Sham, S., Asokan, A., Newmyer, S., Ortiz de Montellano, P. R., and La Mar, G. N. (2002) Influence of the distal His in imparting imidazolate character to the proximal His in heme peroxidase: ^{1}H NMR spectroscopic study of cyanide-inhibited His42-Ala horseradish peroxidase, *J. Am. Chem. Soc. 124*, 11029−11037.

BI060466F